Proceedings of the 7th International Symposium on Cavitation
CAV2009 – Paper No. 79
August 17-22, 2009, Ann Arbor, Michigan, USA

A Panel Method for Trans-Cavitating Marine Propellers

Stefano Gaggero
Marine CFD Group, University of Genova
Italy

Stefano Brizzolara
Marine CFD Group, University of Genova
Italy

ABSTRACT

The extension to super-cavitating propellers of the numerical panel method developed by the Marine CFD Group of the University of Genova is presented and largely validated in the paper.

The validation of the theoretical model for the cavity detachment and closure in the wake of the blade profiles is presented first on a typical super-cavitating profile for which theoretical and experimental solutions are known. Then the 3D panel method is applied on the complete series of Newton-Rader trans-cavitating propeller for which experimental measurements in cavitation tunnel and numerical results obtained by other researchers have been recently published.

The main dynamic characteristics such as thrust and torque coefficients versus the advance ratio and the cavitation index, but also the cavitation patterns, in terms of bubble length at various radii, bubble volume and extension on the trailing vortex wake are presented and discussed for various propellers of the N-R series, having different pitch and expanded area ratios. Good correlations are in general achieved for what regards not only cavitation patterns, but also thrust and torque breakdown consequent to the cavity inception and growth on propeller blades.

INTRODUCTION

The paper presents the latest developments of the propeller boundary element method developed by the Marine CFD group of the University of Genova in its main theoretical and numerical aspects. This development addresses the solution of the super-cavitating propeller problem, i.e. a propeller whose blades are interested by a cavity which also partially extends aft of the blade trailing edge.

The method, in fact, initially developed for subcavitating propellers working in uniform inflow has been refined with several non-linearities, such as exact Kutta condition at trailing edge and adapted trailing vortex wake (Gaggero and Brizzolara (2007) [5]). Subsequently, it has been enhanced to deal with non stationary solutions (Gaggero and Brizzolara, (2008) [6]), relevant for solving the propeller problem working in a ship viscous wake and more recently to allow for a partial sheet cavitation on the face and back of the propeller blades (Gaggero and Brizzolara, (2008) [7]). The capability of the analysis method to accurately capture three dimensional effects of propeller geometry (including the hub) and cavitation effects on the performance can offer interesting opportunities when the method is integrated into an optimization procedure in order to address the problem of automatic refinement of an initial propeller design. Two recent studies (Gaggero and Brizzolara, (2009) [8] Brizzolara, Gaggero, Grasso, (2009) [2]) have shown that the optimization procedure, based on the said panel method, can lead to significant enhancements in terms of propeller efficiency and cavitation volume reduction on the blades.

From the above latest developments, it becomes clear the advantage achievable extending the method to allow for other typologies of propellers, for which conventional lifting line/lifting surface design methods (developed for subcavitating propellers) loose their validity. In this field few very design methods exist, mainly using large approximations and a trial and error procedure from an initial design hypothesis is necessary to obtain the optimum propeller. Among different special propellers, an interesting class is represented by the trans-cavitating and then super-cavitating propellers. Trans-cavitating propellers were at first presented by Newton-Rader and their geometry has several affinities with that of conventional sub-cavitating propellers: blade sections are unconventional foils with rounded leading edge (although with very small curvature radius), cusped trailing edge and the maximum thickness and camber is approximately at mid-chord. These propellers are of interest for applications on medium-sized fast patrol vessels or crafts sailing in excess of 40 knots. At the lowest cavitation indexes (i.e. highest boat speeds) the back of the blade is interested by a full cavity length which extends also in the wake, while at moderate and low speed the behavior of these kind of propellers approaches (also in terms of efficiency) that of conventional propellers. This in opposition with pure supercavitating propellers, whose distinct wedge type profile shape causes rather large drag with consequent loss of efficiency at moderate and low revolutions.

So the first step in this direction, as described in the paper, regards the extension of the mathematical model to allow for the solution of super-cavities in the wake of the profiles. While the solution by panel methods of the partial sheet cavity has been addressed by few research groups (Dang (1999) [3], Vaz

2006 [15], Fine (1992) [4], Kinnas et al. (1999) [11]), the problem of the solution of the (super-)cavity shape in the trailing vortex wake of propeller blade sections is, still, hardly attempted. The method developed by the authors has several affinities with that presented by Young (2002) [18] and Young and Kinnas [16, 19, 20], and applied on similar test cases in (Young, (2008) [17]), especially for the idealization of the cavity model aft of the blade trailing edge. The results presented in the paper, obtained practically for the complete range of Newton-Rader propellers are also compared with these other numerical results, where available.

THEORETICAL AND NUMERICAL MODEL

For the analysis of marine propellers performances, several theoretical and numerical approaches are, nowadays, available. From the 1960's lifting line method, suitable even for the design than for the analysis, to the most recent RANS solvers, different codes have been developed on the basis of different theoretical assumption for the flow field around the propeller. Each of these methods has its own advantages and its own drawback. Lifting line and lifting surface codes, based on the hypothesis of inviscid, irrotational and incompressible fluid, are still the better established methods for the design of a propeller. Potential panel methods, with their capabilities to capture thickness effects and to take into account non linear effects like cavitation (at least sheet cavitation) could be employed for a first tentative analysis in steady and unsteady condition, applying RANS codes (that are still quite demanding in terms of computational resources) to increase accuracy of the performance prediction, visualize viscous effects and further refine the design to achieve better efficiency. The potential panel method steady solution for a propeller can be built (see, for instance Lee, (1987) [9]) considering a right handed propeller rotating with constant angular velocity $\boldsymbol{\omega}$ in a axisymmetric incoming flow field $\boldsymbol{V}_\infty$ (same conclusion can be drawn for the simpler case of a wing subjected to an uniform inflow, neglecting the angular velocity term). In the (x_p, y_p, z_p) coordinate system that rotates with the propeller, the total velocity vector $\boldsymbol{V}$ can be written as the sum of the relative undisturbed inflow $\boldsymbol{V}_{rel}$ (known in the propeller reference system) and the perturbation potential velocity $\boldsymbol{q}_{ind}$, due to the velocity influence of the propeller itself on the velocity field:

$$\boldsymbol{V} = \boldsymbol{V}_{rel} + \boldsymbol{q}_{ind} \tag{1}$$

where the relative velocity $\boldsymbol{V}_{rel}$, in the propeller reference system, can be written as:

$$\boldsymbol{V}_{rel} = \boldsymbol{V}_\infty - \boldsymbol{\omega} \times \boldsymbol{r} \tag{2}$$

With the assumption of an inviscid, irrotational and incompressible fluid, the perturbation velocity can be written in terms of a scalar function, the perturbation potential, that satisfies the Laplace equation:

$$\begin{aligned} \boldsymbol{q}_{ind} &= \nabla\phi \\ \nabla^2\phi &= 0 \end{aligned} \tag{3}$$

By applying Green's second identity for the perturbation potential, the differential problem (3) can be written in integral form with respect to the potential ϕ_p at every point p laying onto the geometry boundaries. The perturbation potential ϕ_i represents the internal perturbation potential, that must be set equal to zero in order to simulate fluid at rest inside the boundaries of all the bodies subject to the external inflow (blades, hub, wing).

$$\begin{aligned} 2\pi\phi_p &= \int_{S_B+S_{CB}} \left[\phi_q - \phi_{qi}\right] \frac{\partial}{\partial \boldsymbol{n}_q} \frac{1}{r_{pq}} dS \\ &- \int_{S_B+S_{CB}} \left[\frac{\partial \phi_q}{\partial \boldsymbol{n}_q} - \frac{\partial \phi_{qi}}{\partial \boldsymbol{n}_q}\right] \frac{1}{r_{pq}} dS \\ &+ \int_{S_W} \Delta\phi_q \frac{\partial}{\partial \boldsymbol{n}_q} \frac{1}{r_{pq}} dS \end{aligned} \tag{4}$$

The subscript q corresponds to the variable point in the integration, $\boldsymbol{n}$ is the unit normal to the boundary surfaces and r_{pq} is the distance between points p and q.

Equation (4) is a Fredholm integral equation and expresses the potential on the propeller blade as a superposition of the effects induced by a continuous distribution of sources on the blade and hub surfaces and a continuous distribution of dipoles (whose strength is equal to the potential itself in that point) on the blade, hub and wake surfaces that can be calculated, directly, via boundary conditions, or, indirectly, inverting equation (4).

For the solution of equation (4) a certain number of boundary conditions must be applied. The choice of the boundary conditions depends on the kind of the problem to be solved. On the wetted part of the body (the wing or the blades plus the hub not subjected to cavitation, i.e. not subjected to a pressure below the vapour tension) the kinematic boundary condition holds (the flow must be tangent to the body surface) and allows to define the source strengths in terms of the known inflow velocity relative to the propeller reference system:

$$\frac{\partial \phi_q}{\partial n_q} = -\boldsymbol{V} \cdot n_q \tag{5}$$

At the blade trailing edge the Kutta condition states that the flow must leave with a finite velocity or that the pressure jump at the blade trailing edge must be zero. In a steady problem, the Kutta condition allows to write the dipole intensities, constant along each streamlines (equivalent to each chordwise strip in the discretized formulation), on the wake, first, applying the "linear" Morino (Morino, 1974 [10]) Kutta condition:

$$\Delta\phi_{T.E.} = \phi^U_{T.E.} - \phi^L_{T.E.} + \boldsymbol{V}_{rel} \cdot \boldsymbol{r}_{T.E.} \tag{6}$$

where the sup scripts U and L stand for the upper and the lower face of the trailing edge. After, the zero pressure jump can be achieved via an iterative scheme. In fact the pressure difference at trailing edge (or the pressure coefficient difference) at each m streamlines (or at each m blade strip for

the discretized problem) is a non linear function of dipole intensities on the blade:

$$\Delta p_m(\phi) = p_m^U(\phi) - p_m^L(\phi) \tag{7}$$

So, an iterative scheme is required to force a zero pressure jump, working on dipoles strength on the blade (and, consequently, on potential jump on the trailing wake). By applying a Newton – Raphson scheme with respect to the potential jump on the wake $\Delta\phi$, equal in the steady problem to the potential jump at blade trailing edge, the wake potential jump is given by:

$$\{\Delta\phi\}^{k+1} = \{\Delta\phi\}^k - \left[J^k\right]^{-1}\{\Delta p(\phi)\}^k \tag{8}$$

where the index k denotes the iteration, $\left[\Delta p(\phi)\right]^k$ is the pressure jump at trailing edge obtained solving the problem at iteration k (corresponding to the $\Delta\phi^k$ solution) and $\left[J^k\right]$ is the Jacobian matrix numerically determined (9):

$$J_{ij}^k = \frac{\partial \Delta p_i^k}{\partial \Delta \phi_j^k} \tag{9}$$

while, for the first iteration, the solution $\Delta\phi^k$ and the corresponding pressure jump is taken from the linear Morino solution (6).

Moreover the wake should be a streamsurface: the zero force condition is satisfied when the wake surface is aligned with the local velocity vector. In the present method this condition is only approximated and the wake surface is assumed frozen and laying on an helicoidal surface whose pitch is equal to the blade pitch. Assuming that the influence of the cavity bubble is small in the definition of the wake surface, an approach similar to that proposed by Gaggero and Brizzolara, (2007) [5] can be adopted and the cavity solver could be improved using the aligned wake calculated for the steady non cavitating flow.

Analogous (kinematic and dynamic) boundary conditions have to be forced on the body cavitating surfaces, in order to solve for the singularities (sources and dipoles) distributed there (Caponnetto and Brizzolara, 1995 [1], Fine (1992) [4], Mueller and Kinnas, (1999) [11], Young and Kinnas, (2001) [16], Vaz and Bosschers, (2006) [15]).

Different approaches are possible: a fully linear approach, in which cavity velocities can be considered enough small to allow linearization of boundary conditions or a fully nonlinear one, in which singularities are located on the cavity surface that need to be found iteratively. On the other hand, an intermediate approach, the partial nonlinear approach, can be adopted, in order to take into account the weakly nonlinearity of the boundary conditions (the dynamic boundary condition on the cavitating part of the blade and the closure condition at its trailing edge) without the need to collocate the singularities on the effective cavity surface. If the cavity thickness can be considered enough small with respect to the chord, singularities can be placed on the body surface and problem nonlinearity can be solved with this assumption (see, for instance, figure 1).

On the cavity surface S_{CB} the pressure must be constant and equal to the vapour pressure or the modulus of the velocity, obtained via Bernoulli's equation, must be equal to the total velocity V_{Vap} on the cavity surface.

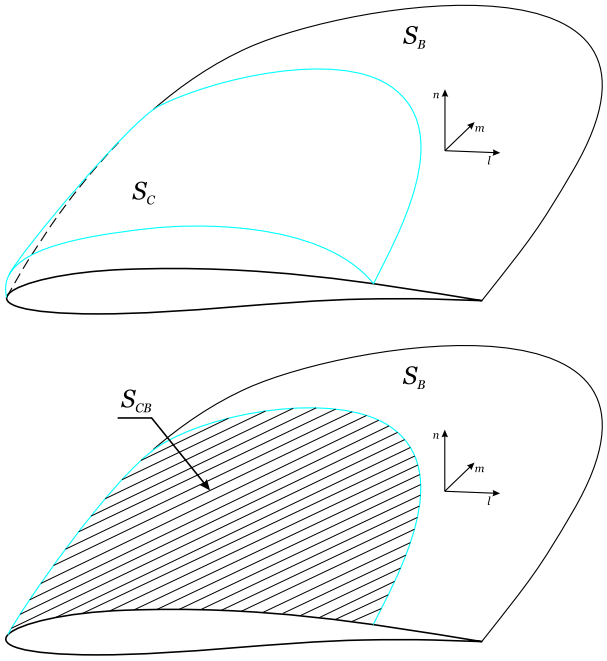

Figure 1: Exact (S_C) and approximate (S_{CB}) cavity surface definition.

If p_∞ is the pressure of the undisturbed flow field, p is the actual pressure and ρ is the flow density, in a propeller fixed reference system, Bernoulli's equation can be written in the following form:

$$p_\infty + \frac{1}{2}\rho|\boldsymbol{V}_\infty|^2 = p + \frac{1}{2}\rho\left[|\boldsymbol{V}|^2 - |\boldsymbol{\omega}\times\boldsymbol{r}|^2\right] + g y_{shaft} \tag{10}$$

If p_{Vap} indicates the vapour pressure of the flow, the modulus of the corresponding vapour pressure V_{Vap}, via equation (10) on the cavity surface, along each section of constant radius, , is equal to:

$$|\boldsymbol{V}_{Vap}| = \sqrt{\frac{2}{\rho}\left(p_\infty - p_{Vap}\right) + |\boldsymbol{V}_\infty|^2 + |\boldsymbol{\omega}\times\boldsymbol{r}|^2 - 2 g y_{shaft}} \tag{11}$$

This dynamic boundary condition can be written as a Dirichlet boundary condition for the perturbation potential.

In order to obtain a Dirichlet boundary condition from the dynamic boundary condition it is necessary, first, (following Brizzolara and Caponnetto, (1995) [1]) to define the controvariant components V^α and the covariant components V_β of the velocity vector $\boldsymbol{V}$:

$$\begin{aligned} &\boldsymbol{V} = V^\alpha \boldsymbol{e}_\alpha \\ &V_\beta = \boldsymbol{V}\cdot\boldsymbol{e}_\beta \rightarrow V_\beta = V^\alpha \boldsymbol{e}_\alpha \cdot \boldsymbol{e}_\beta \end{aligned} \tag{12}$$

where $\boldsymbol{e}_\alpha$ are the unit vector of the reference system and α, β are equal to 1, 2 and 3. Defining the square matrix $g_{\alpha\beta} = \boldsymbol{e}_\alpha \cdot \boldsymbol{e}_\beta$ and its inverse $g^{\alpha\beta}$, the covariant component can be written as:

$$\begin{aligned} V_\alpha &= V^\beta g_{\alpha\beta} \\ V_\alpha g^{\alpha\gamma} &= V^\beta g_{\alpha\beta} g^{\alpha\gamma} = V^\gamma \end{aligned} \tag{13}$$

Combining equations (12) with equations (13) the velocity vector $\boldsymbol{V}$ can be expressed in terms of the covariant components:

$$\boldsymbol{V} = g^{\alpha\beta} V_\alpha \boldsymbol{e}_\beta \tag{14}$$

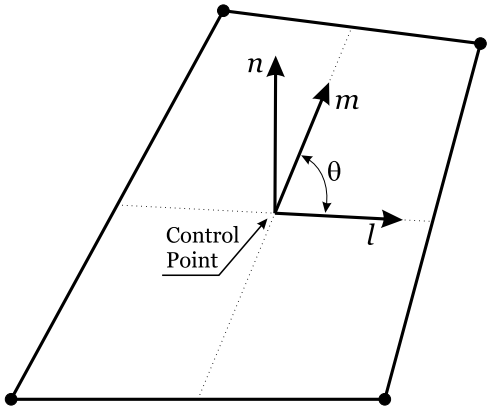

Figure 2: local non orthogonal panel coordinate system. Vectors ***l*** and ***m*** are formed by the lines connecting panel sides midpoints. Vector ***n*** is normal to ***l*** and ***m***.

In the present case (figure 2) the local coordinate system is defined by the vectors **l**, **m** and **n**, where $\boldsymbol{l} \cdot \boldsymbol{m} = \cos\theta$, $\boldsymbol{l} \cdot \boldsymbol{n} = 0$ and $\boldsymbol{m} \cdot \boldsymbol{n} = 0$. The $g_{\alpha\beta}$ and the $g^{\alpha\beta}$ matrix can, thus, be written in the following form:

$$\begin{aligned} g_{xy} &= \begin{bmatrix} 1 & \cos\theta & 0 \\ \cos\theta & 1 & 0 \\ 0 & 0 & 1 \end{bmatrix} \\ g^{xy} &= \frac{1}{\sin^2\theta} \begin{bmatrix} 1 & -\cos\theta & 0 \\ -\cos\theta & 1 & 0 \\ 0 & 0 & \sin^2\theta \end{bmatrix} \end{aligned} \tag{15}$$

while the expression of the gradient can be obtained, from (14) and (15), as:

$$\nabla = \frac{1}{\sin^2\theta} \begin{bmatrix} 1 & -\cos\theta & 0 \\ -\cos\theta & 1 & 0 \\ 0 & 0 & \sin^2\theta \end{bmatrix} \begin{Bmatrix} \partial/\partial l \\ \partial/\partial m \\ \partial/\partial n \end{Bmatrix} \tag{16}$$

The covariant component of the velocity on the non orthogonal reference system can be expressed as:

$$\begin{aligned} V_l &= \boldsymbol{V}_{rel} \cdot \boldsymbol{l} + \frac{\partial\phi}{\partial l} = U_l + \frac{\partial\phi}{\partial l} \\ V_m &= \boldsymbol{V}_{rel} \cdot \boldsymbol{m} + \frac{\partial\phi}{\partial m} = U_m + \frac{\partial\phi}{\partial m} \\ V_n &= \boldsymbol{V}_{rel} \cdot \boldsymbol{n} + \frac{\partial\phi}{\partial n} = U_n + \frac{\partial\phi}{\partial n} \end{aligned} \tag{17}$$

And, from equation (14) the velocity vector is given by:

$$\begin{aligned} \boldsymbol{V} &= \left(\frac{1}{\sin^2\theta} (V_l - V_m) \cos\theta \right) \boldsymbol{l} \\ &+ \left(\frac{1}{\sin^2\theta} (V_m - V_l) \cos\theta \right) \boldsymbol{m} \\ &\quad V_n \boldsymbol{n} \end{aligned} \tag{18}$$

Assuming V_n vanishingly small, the normal component of the velocity can be neglected: in general it deteriorates the robustness of the solution and hardly influences the cavity extent as demonstrated by Fine (1992) [4].

Thus the modulus of the velocity becomes:

$$|\boldsymbol{V}|^2 = V_\alpha V_\beta g^{\beta\alpha} = \frac{1}{\sin^2\theta} \left(V_l^2 + V_m^2 - 2 V_l V_m \cos\theta \right) \tag{19}$$

Considering ***l*** approximately aligned with the local surface flow, it is possible to solve (19) with respect to $\partial\phi/\partial l$ (because, from equation (17) $V_l = U_l + \partial\phi/\partial l$) obtaining:

$$\begin{aligned} \frac{\partial\phi}{\partial l} &= -U_l + \left(\frac{\partial\phi}{\partial m} + U_m \right) \cos\theta \\ &+ \sin\theta \sqrt{|\boldsymbol{V}|^2 - \left(\frac{\partial\phi}{\partial m} + U_m \right)^2} \end{aligned} \tag{20}$$

Equation (20) can be integrated to finally achieve a Dirichlet boundary condition for the perturbation potential, equivalent to the dynamic boundary condition. On the cavitating surface, where $\boldsymbol{V} = \boldsymbol{V}_{Vap}$, equation (20), after integration between bubble leading edge and bubble trailing edge, yields to:

$$\begin{aligned} \phi(m,l) = \; & \phi_0(m) + \int_{L.E._{Bub}}^{T.E._{Bub}} \left[-U_l + \left(\frac{\partial\phi}{\partial m} + U_m \right) \cos\theta \right. \\ & \left. + \sin\theta \sqrt{|\boldsymbol{V}_{Vap}|^2 - \left(\frac{\partial\phi}{\partial m} + U_m \right)^2} \right] dl \end{aligned} \tag{21}$$

where the only unknowns are the values of the perturbation potential at the bubble leading edge.

The kinematic boundary condition on the cavity surface, in steady flow, requires the flow to be tangent to the cavity surface itself.

With respect to the local (***l***,***m***,***n***) orthogonal coordinate reference system (figure 2), the cavity surface S_C (in terms of its thickness t) is defined as:

$$\boldsymbol{n} = t(\boldsymbol{l},\boldsymbol{m}) \rightarrow \boldsymbol{n} - t(\boldsymbol{l},\boldsymbol{m}) = 0 \tag{22}$$

and the tangency condition, by applying the covariant and the controvariant representation of velocity vectors and gradient defined above, can be written as:

$$\begin{aligned} \boldsymbol{V}\cdot\nabla\left(\boldsymbol{n}-t(\boldsymbol{l},\boldsymbol{m})\right) &= 0 \\ V_\alpha\nabla^\alpha\left(\boldsymbol{n}-t(\boldsymbol{l},\boldsymbol{m})\right) &= 0 \\ g^{\alpha\beta}V_\alpha\nabla_\beta\left(\boldsymbol{n}-t(\boldsymbol{l},\boldsymbol{m})\right) &= 0 \end{aligned} \tag{23}$$

Moreover:

$$\begin{aligned} \frac{\partial}{\partial l}\left(\boldsymbol{n}-t(\boldsymbol{l},\boldsymbol{m})\right) &= -\frac{\partial t}{\partial l} \\ \frac{\partial}{\partial m}\left(\boldsymbol{n}-t(\boldsymbol{l},\boldsymbol{m})\right) &= -\frac{\partial t}{\partial m} \\ \frac{\partial}{\partial n}\left(\boldsymbol{n}-t(\boldsymbol{l},\boldsymbol{m})\right) &= 1 \end{aligned} \tag{24}$$

And, from equation (16) and (23):

$$\frac{1}{\sin^2\theta}\{V_l,V_m,V_n\}\cdot \begin{bmatrix} 1 & -\cos\theta & 0 \\ -\cos\theta & 1 & 0 \\ 0 & 0 & \sin^2\theta \end{bmatrix}\cdot\begin{Bmatrix} -\partial t/\partial l \\ -\partial t/\partial m \\ 1 \end{Bmatrix} = 0 \tag{25}$$

Equation (25) yields to a differential equation for cavity thickness over the blade, with respect to the local reference system:

$$\begin{aligned} &\frac{\partial t}{\partial l}\left[\left(U_m+\frac{\partial\phi}{\partial m}\right)\cos\theta-\left(U_l+\frac{\partial\phi}{\partial l}\right)\right] + \\ &\frac{\partial t}{\partial m}\left[\left(U_l+\frac{\partial\phi}{\partial l}\right)\cos\theta-\left(U_m+\frac{\partial\phi}{\partial m}\right)\right] + \\ &\sin^2\theta\left(U_n+\frac{\partial\phi}{\partial n}\right) = 0 \end{aligned} \tag{26}$$

To solve for the cavity planform shape, another condition is required on the cavitating surface: the cavity height at its trailing edge must be zero (cavity closure condition).

This determines the necessity of an iterative solution to satisfy this, further, condition because the cavity height, computed via equation (26) is a non linear function of the solution (the perturbation potential ϕ) and of the extent of the cavity surface (via the dynamic boundary condition):

$$t(l_{T.E.}) = 0 \tag{27}$$

If the cavity thickness at the blade trailing edge is different from zero (this is a common situation, specially near the tip for propellers working at low values of cavitation index and for propeller geometries specifically designed to deal with these phenomena), the blade can be considered as supercavitating.

Considering the wake geometry as a force free invariant surface coincident with the steady non cavitating flow wake obtained with the circumferential averaged inflow, with the assumption that the upper and lower sides of the supercavity downstream the trailing edge collapse into a single surface the linearized S_{CW} surface on which the kinematic and dynamic boundary conditions have to be forced can be taken as the zero thickness trailing wake sheet itself. With these assumption, the integral problem (4) can be rewritten discriminating between field points on the solid surfaces (blades and hub) and points on the wake.

For a point on the solid surfaces (wetted or cavitating):

$$\begin{aligned} 2\pi\phi_p &= \int_{S_B+S_{CB}}\phi_q\frac{\partial}{\partial\boldsymbol{n}_q}\frac{1}{r_{pq}}dS \\ &- \int_{S_B+S_{CB}}\frac{\partial\phi_q}{\partial\boldsymbol{n}_q}\frac{1}{r_{pq}}dS \\ &- \int_{S_{CW}}\left(\frac{\partial\phi_q^+}{\partial\boldsymbol{n}_q}-\frac{\partial\phi_q^-}{\partial\boldsymbol{n}_q}\right)\frac{1}{r_{pq}}dS \\ &+ \int_{S_W+S_{CW}}\Delta\phi_q\frac{\partial}{\partial\boldsymbol{n}_q}\frac{1}{r_{pq}}dS \end{aligned} \tag{28}$$

For a point of the wake supercavitating surface, after the desingularization proposed by Fine (1992) [4], the potential ϕ^+ on the upper side of the wake cavitating surface (at this point only back supercavitation is taken into account) is expressed by:

$$\begin{aligned} 4\pi\phi_p^+ &= \int_{S_B+S_{CB}}\phi_q\frac{\partial}{\partial\boldsymbol{n}_q}\frac{1}{r_{pq}}dS \\ &- \int_{S_B+S_{CB}}\frac{\partial\phi_q}{\partial\boldsymbol{n}_q}\frac{1}{r_{pq}}dS \\ &- \int_{S_{CW}}\left(\frac{\partial\phi_q^+}{\partial\boldsymbol{n}_q}-\frac{\partial\phi_q^-}{\partial\boldsymbol{n}_q}\right)\frac{1}{r_{pq}}dS \\ &+ \int_{S_W+S_{CW}}\Delta\phi_q\frac{\partial}{\partial\boldsymbol{n}_q}\frac{1}{r_{pq}}dS \\ &+ 2\pi\Delta\phi_q \end{aligned} \tag{29}$$

in which the jump of the derivatives of the potential with respect to the normal direction on the wake cavitating surface (in the following referenced as σ_W) represents a source distribution responsible of the cavity thickness aft the blade trailing edge.

In the same way as previously done for the dynamic and kinematic boundary conditions on the cavitating region on the blade, an expression is needed for the Dirichlet type condition for ϕ^+ and for the cavity thickness t_w on the wake.

As in Fine, (1992) [4], an orthogonal reference system (***s,u,n***), whose ***s*** unit vector is aligned with the mean flow

velocity on the wake, has been defined and the normal component of the velocity has been neglected for the same solution stability reasons observed for the blade cavitating surfaces. The Dirichlet boundary condition becomes:

$$\phi(s,u) = \phi(m, l_{Blade\,Trailing\,Edge}) + \int_{Blade\,T.E.}^{Bubble\,T.E.} -U_s + \sqrt{\left|\boldsymbol{V}_{Vap}\right|^2 - U_v^{\,2}} \tag{30}$$

In which also the wake cross flow terms U_v, whose influence was found to be small (as demonstrated by Fine, (1992) [4]) can be neglected. The term $\phi(m, l_{Blade\,Trailing\,Edge})$ is the value of the potential at the blade trailing edge on a supercavitating region, computed using equation (21) from the bubble leading edge to the blade trailing edge.

Rearranging the kinematic boundary condition, an expression for the cavity thickness on the wake can be obtained. Following the work by Fine (1992) [4] and by Vaz (2006) [15], the cavity thickness solves, on the local orthogonal reference system, the differential equation:

$$\left(\sqrt{\left|\boldsymbol{V}_{Vap}\right|^2 - U_v^{\,2}}\right)\frac{\partial t_W}{\partial s} = \sigma_W \tag{31}$$

plus another differential equation concerning the cavity camber over the wake surface:

$$\left(\sqrt{\left|\boldsymbol{V}_{Vap}\right|^2 - U_v^{\,2}}\right)\frac{\partial C_W}{\partial s} = 0 \tag{31}$$

for which the initial conditions are set from the cavity thickness at the blade trailing edge:

$$\begin{aligned} t_W(s=0) &= t(l_{T.E.}) \\ C_W(s=0) &= \frac{1}{2}t(l_{T.E.}) \end{aligned} \tag{32}$$

Another aspect concerning propeller cavitation that must be taken into account is midchord cavitation that is becoming common in recent designs: it is due to the attempt to increase efficiency, to the fact that, often, new design sections have flat pressure distributions on the suction side, or to the fact that a conventional propeller works in off design condition (Young and Kinnas, (2001) [16], Mueller and Kinnas, (1999) [11]).

The non axisymmetric flow a propeller may experience inside a wake is, often, characterized by higher incoming velocities at certain angular positions with respect to the mean inflow considered, for instance, for the design: this traduces in small or negative angles of attack that may lead to face cavitation.

In order to capture simultaneously face and back cavitation and to allow midchord detachment, the theoretical formulation is exactly the same explained above with reference to the more common case of back cavitation only. The face cavitation problem can be treated exactly as the back cavitation problem, thus defining and adequate reference system (the face non orthogonal reference system needs to have the corresponding ***l*** unit vector pointing along the versus of the tangential velocity on the face of the profile) and imposing the same dynamic, kinematic and cavity closure conditions with respect to this, new, local reference system (figure 3).

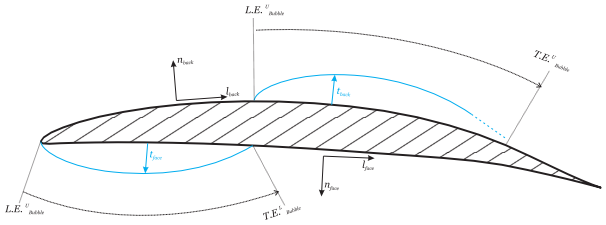

Figure 3: Back and Face reference coordinate system.

Arbitrary detachment line can be found, iteratively, applying a criteria equivalent, in two dimensions, to the Villat-Brillouin cavity detachment condition (as in Young and Kinnas, (2001) [16], Mueller and Kinnas, (1999) [11]). Starting from a detachment line obtained from the initial wetted solution (and identified as the line that separates zones with pressures higher than the vapour tension from zones subjected to pressure equal or lower pressures) or an imposed one (typically the leading edge), the detachment line is iteratively moved according to:

- If the cavity at that position has negative thickness, the detachment location is moved toward the trailing edge of the blade.
- If the pressure at a position upstream the actual detachment line is below vapour pressure, then the detachment location is moved toward the leading edge of the blade.

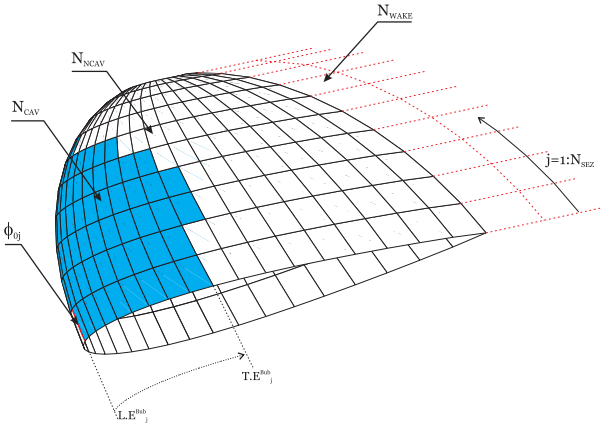

Figure 4: Blade numbering arrangement

Equation (4) (in the case of partial cavitation) or equations (28) and (29) (in the case of supercavitation) are second kind Fredholm integral equations for the perturbation potential ϕ. Numerically they can be solved approximating boundary surfaces with quadrilateral or hyperboloidal panels (Morino, (1974) [10]), substituting integrals with discrete sums and imposing the appropriate boundary conditions. The panel arrangement selected for this problem is the same adopted for

the steady propeller panel method (Gaggero and Brizzolara, (2007) [5]), with all the surfaces discretized with panair like panels (each one composed by five flat subpanel) and with hyperboloidal panels (recently adopted in order to save computational time and achieve the same order of accuracy).

For the partial cavitating condition and with respect to the blade numbering convention of figure 4, the linear system that solves equation 28 for the key blade (all the other blades, in the steady solution, are taken into account only via influence coefficients) becomes:

$$\begin{aligned}\sum_{j=1}^{N_{NCAV}} A_{ij}\mu_j + \sum_{j=1}^{N_{CAV}} B_{ij}\sigma_j^{cav.} + \sum_{j=1}^{N_{SEZ}} \phi_{0j}\xi_j \left[\sum_{m=L.E._j^{Bub.}}^{T.E._j^{Bub.}} A_{ij} \right] = \\ \sum_{j=1}^{N_{NCAV}} B_{ij}\sigma_j + \sum_{j=1}^{N_{SEZ}} \xi_j \left[\sum_{m=L.E._j^{Bub.}}^{T.E._j^{Bub.}} F_{ij}A_{ij} \right] + \sum_{j=1}^{N_{WAKE}} W_{ij}\Delta\phi_j\end{aligned} \tag{33}$$

where ξ_j is a cavitation index: if the j section is subjected to cavitation ξ_j is equal to 1, otherwise ξ_j is equal to 0.

For the supercavitating case, only minor modification are required, as for instance presented by Fine, (1992) [4]. The linear system has to satisfy the integral equation for the field points on the solid surfaces and for the field points on the wake surfaces, together with Dirichlet boundary conditions extended, with equation (30), along mean flow direction on the wake. From this point of view the parameter F_{ij} that appears on the linear system represents the value of the integral of equations (21) or (30) computed via a quadrature technique, while ϕ_{0j} represents the known (calculated via extrapolation) value of the perturbation potential at the leading edge of each cavitating strip of the discretized problem.

To find the correct discrete cavity planform it is necessary to impose the cavity closure condition and an iterative approach is needed because of the nonlinear dependency between the cavity thickness and the dynamic boundary condition.

First, the linear system (33) is solved with a first guessed cavity planform (generally selected, from the fully wetted solution, as the set of panels subjected to a pressure below the vapour tension) and all the unknowns (dipoles, sources and cavity thickness) are computed with the current configuration of cavitating and non cavitating panels. With this first guessed cavity shape the closure condition, normally, is not satisfied. Hence, the shape is iteratively changed, adding (if the cavity thickness is still positive) or subtracting (if the cavity thickness is already negative), at the trailing edge of each cavitating section, a panel, and solving again the problem, with the new configuration of cavitating and non cavitating panels, until the cavity thickness at the bubble trailing edge is below a fixed threshold and, simultaneously, the derivative of cavity thickness at the same point with respect to the chordwise coordinate is negative (in order to select the stable solution). If more than a cavitating strip has a cavity thickness greater than zero at the blade trailing edge (when there is only one cavitating strip extended till the blade trailing edge, generally this section is that at tip, that is characterized by tip vortex cavitation that should be treated adequately), with the same criteria (cavity thickness below a certain threshold and negative cavity thickness derivative) the problem is solved again guessing an extension of the cavity on the wake and iterating until convergence.

RESULTS

For the validation of the developed numerical code, a series of computation has been carried out in order to check the ability to capture back and face cavitation, together with the convergence of the cavity bubble when it develops aft the blade trailing edge. The numerical validation of the method has been performed on the numerical results performed by Young and Liu, (2008) [17] with an affine panel method.

A rectangular hydrofoil, with aspect ratio equal to 4, with a NACA 66 profile at 0° angle of attack has been computed in super-cavitating condition (σ_V = 0.24), with an increasing number of panels on the blade and on the wake. Eight different mesh densities have been considered. First the code has been tested for the convergence of the cavity shape changing the number of panels on the blade (15 fixed sections along the span and from 30 to 60 panels along the chord with a fixed value of panels on each wake strip equal to 100) and, after, with the finest grid, the mesh density in the wake has been changed (from 100 to 400 panels per strip), as presented in figure 6.

The convergence of the solution, as shown, is good: the face cavity detaches from the leading edge (the 4% of chord camber determines, at 0° angle of attack, the inversion at leading edge of the pressure distribution), while the back cavity detaches almost at midchord, in accordance with the fully wetted pressure distribution presented for the section at midspan of the wing in figure 5.

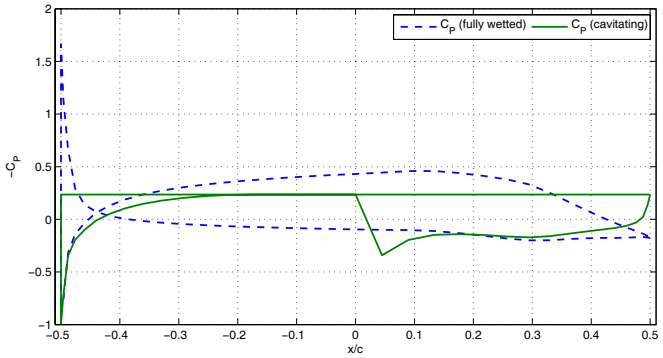

Figure 5: Pressure distribution for the rectangular wing at midsection, NACA66 profile, t/c = 0.06, f/c = 0.04 α = 0° at σ_V = 0.24. Comparison between fully wetted solution and converged cavity solution.

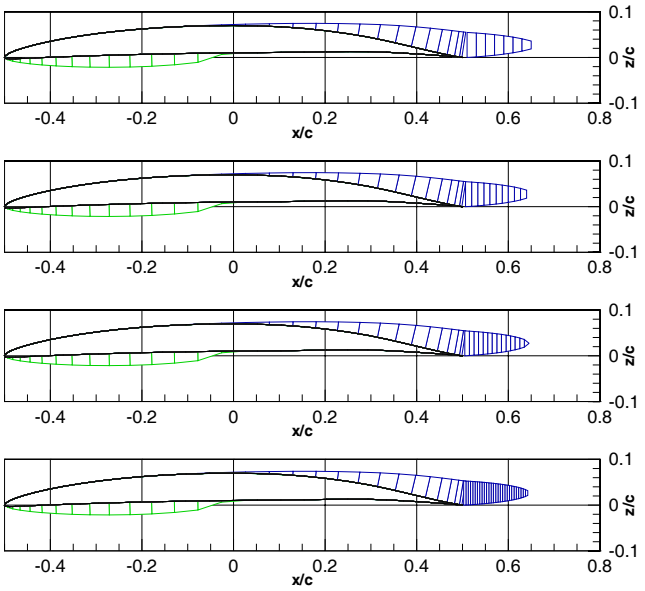

Figure 6: Face and back cavitation, rectangular wing at midsection, NACA66 profile, t/c = 0.06, f/c = 0.04 $\alpha = 0°$ at $\sigma_V = 0.24$. Convergence with number of panels on wake (100 top – 400 bottom).

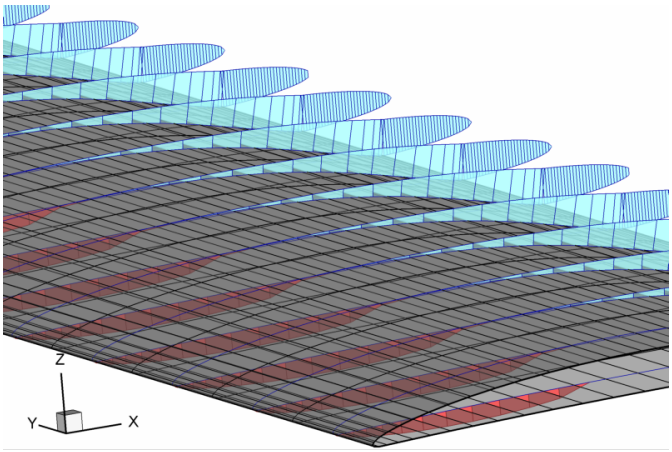

Figure 7: Face and back cavitation, on the rectangular wing, NACA66 profile, t/c = 0.06, f/c = 0.04 $\alpha = 0°$ at $\sigma_V = 0.24$.

In the case of propellers, a custom propeller, named E033, has been selected to analyze the performances of the numerical code. E033 is a four bladed CP propeller designed for high speed (35 knots) displacement vessels with a lifting surface code, allowing for partial cavitation at lowest cavitation indexes. It has a pitch ratio P/D=1.5 at r/R = 0.7, an expanded area ratio of A_E/A_0=0.685 and standard NACA16 profiles. A wide series of experiments is available for this propeller in cavitating conditions, including thrust and torque measurements and cavity sketches and photos, directly measured at the cavitation tunnel of the University of Genova.

The prediction of the cavity planform seems to be quite accurate. Figure 8 compares the experimental cavity planform with that computed on the suction side of the blade in the case of the propeller operating in an uniform axisymmetric inflow. Figure 9, moreover, presents the numerical computation of the cavity planform highlighting its behavior on the wake, aft the blade trailing edge. Except the region near the tip (that is subjected to a strong tip vortex cavitation that the numerical method is still not able to compute) the agreement is good. The region near the blade tip is characterized by supercavitation mixed with the tip vortex: numerically, neglecting the last tip section, also these features are captured, at least in terms of supercavity "inception". The propeller performances, like thrust and torque and their breakdown lowering the cavitation index are themselves well captured for a large set of different working condition, as for instance presented in Gaggero and Brizzolara (2008) [7] and (2009) [8].

The Newton-Rader propellers (Newton and Rader, (1961) [12]) represent one of the possible solution to achieve multispeed performance without significant losses of efficiency between wetted and supercavitating conditions and thus, are optimal candidates to test the capabilities of the numerical code and to validate it in order to perform further analysis and designs computations. The Newton-Rader series is composed by twelve methodically varied three bladed propellers (diameter equal to 0.254m), that cover pitch ratios between 1.0 and 2.0, and blade area ratio from 0.48 to 0.95. All the propellers have been obtained varying systematically the geometry of a parent propeller, characterized by a pitch over diameter ratio equal to 1.25, by a blade area ratio equal to 0.71 and designed for an advance coefficient of 0.993. This parent propeller, from its original design, had been modified two times at the leading edge, flattening the camber line, to avoid face cavitation that characterized the original design at high values of advance coefficient and these modifications have been, after, applied to all the twelve designs.

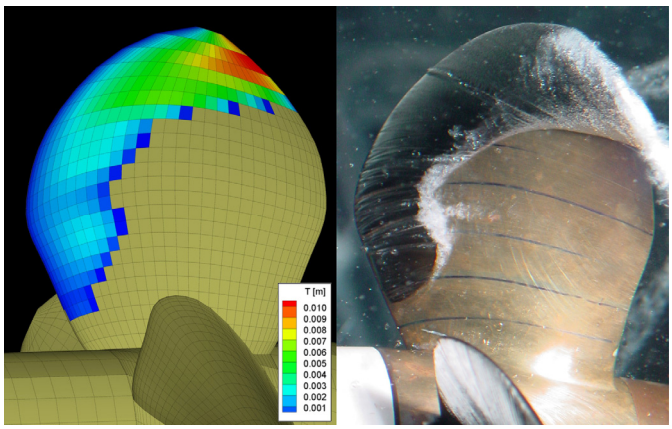

Figure 8: Propeller E033, cavity planform J = 0.8, $\sigma_N = 2.5$ (colours represent cavity thickness).

For these propellers a huge amount of data is available, obtained at the Vosper Cavitation Tunnel by R.N. Newton and H.P. Rader and published for the Quarterly Transactions of the Royal Institution of Naval Architects in 1961. For all the twelve propellers the original work by Newton and Rader, (1962) [12] presents the thrust, the torque and the efficiency coefficients for nine different cavitation numbers at rate of advance intervals $\Delta J = 0.05$ together with photographs showing the cavitation patterns at various working conditions. Unfortunately, the

quality of the original images on the copy of the work available at the University of Genova library is quite poor, so no direct comparisons of cavity planform have been presented in the current work and only qualitative remarks and comparisons with other numerical calculations have been considered.

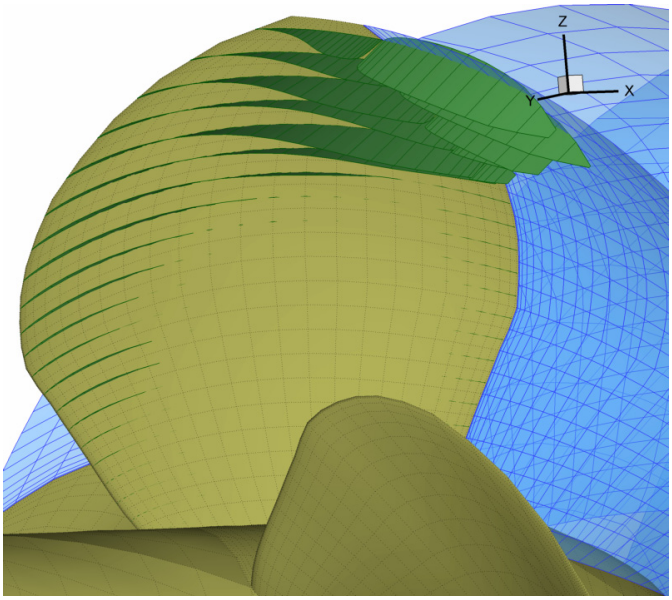

Figure 9: Propeller E033, supercavitating pattern J = 0.8, σ_N = 2.5.

Almost all the propellers of the series have been tested. For all the cases the results have been obtained discretizing the propeller blade with 16 sections along the radius and 25 panels along the chord (both for face and back), with the vortex trailing wake extending for about three complete revolutions aft the blade trailing edge. With the numbering convention proposed by Newton and Rader, numerical values of thrust and torque have been computed for propellers A3/48/167, A3/48/206, A3/71/125, A3/71/166, A3/71/206, A3/95/124, A3/95/165 and A3/95/204. The attention, in particular, has been focused on propellers A3/71/125 (the parent propeller) and A3/95/124, tested at three different advance coefficients around the design one (0.9, 1.0 and 1.1), for which other numerical computations (from Young and Liu, (2008) [17]) are available.

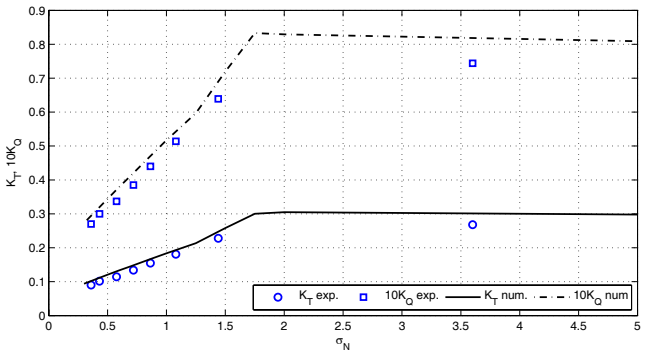

Figure 10: Newton Rader 048, P/D 1.67, J = 1.2

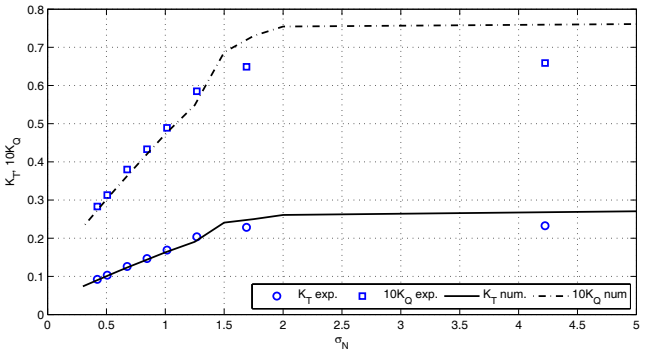

Figure 11: Newton Rader 048, P/D 1.67, J = 1.3

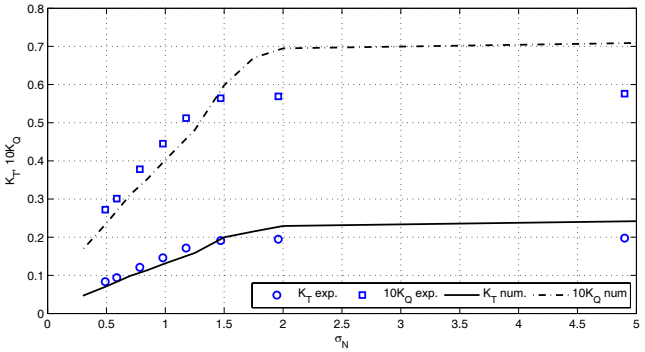

Figure 12: Newton Rader 048, P/D 1.67, J = 1.4

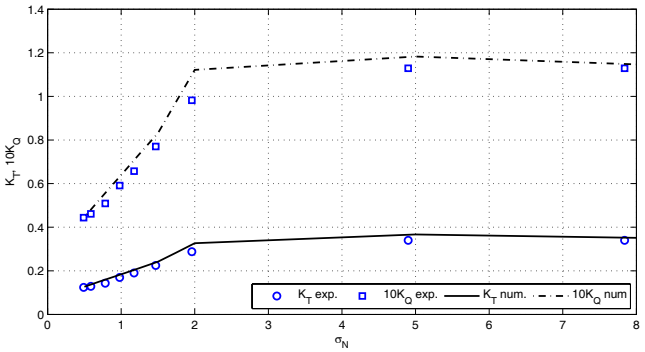

Figure 13: Newton Rader 048, P/D 2.06, J = 1.4

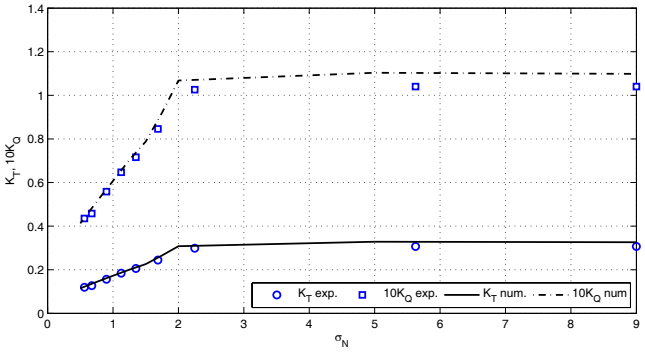

Figure 14: Newton Rader 048, P/D 2.06, J = 1.5

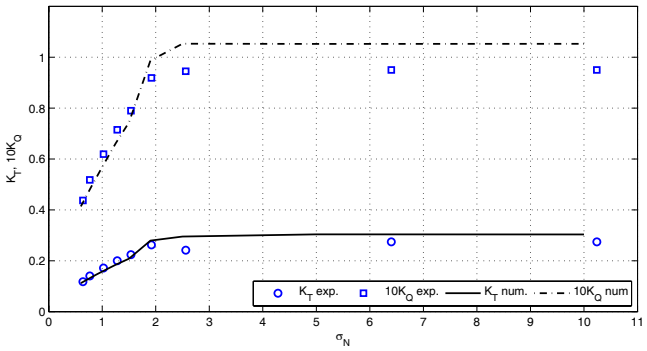

Figure 15: Newton Rader 048, P/D 2.06, J = 1.6

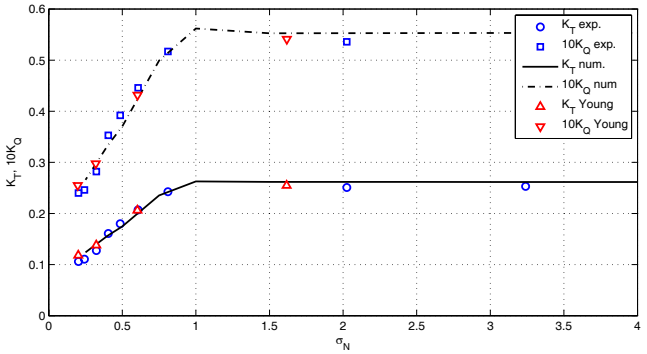

Figure 16: Newton Rader 071, P/D 1.25, J = 0.9

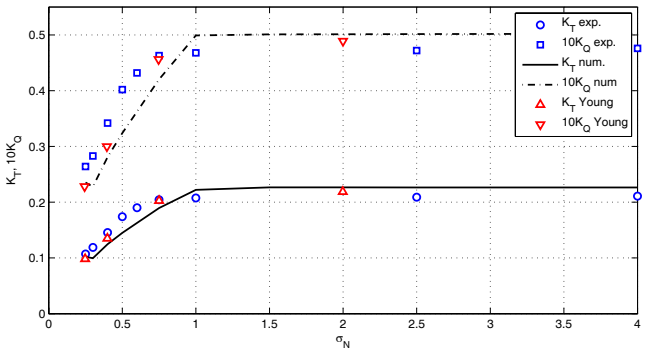

Figure 17: Newton Rader 071, P/D 1.25, J = 1.0

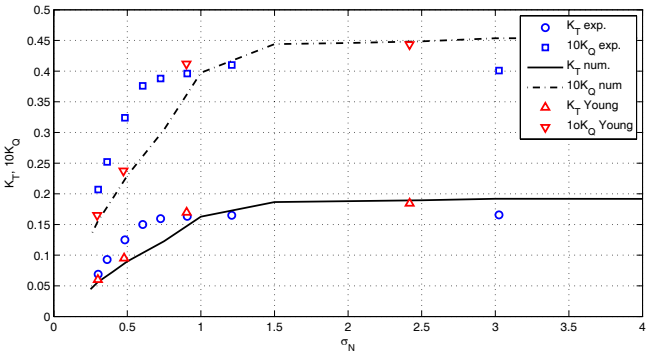

Figure 18: Newton Rader 071, P/D 1.25, J = 1.1

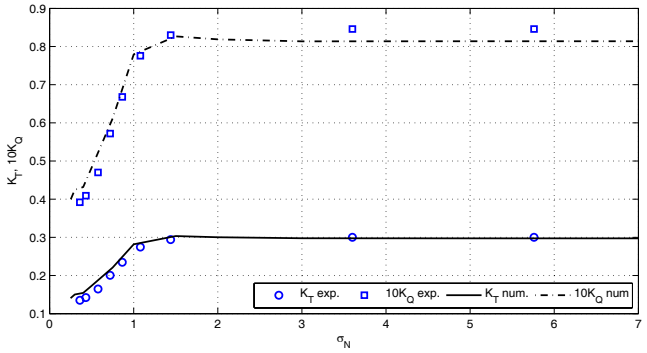

Figure 19: Newton Rader 071, P/D 1.66, J =1.2

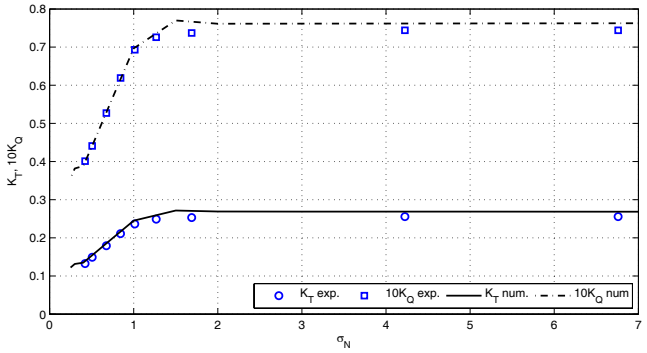

Figure 20: Newton Rader 071, P/D 1.66, J =1.3

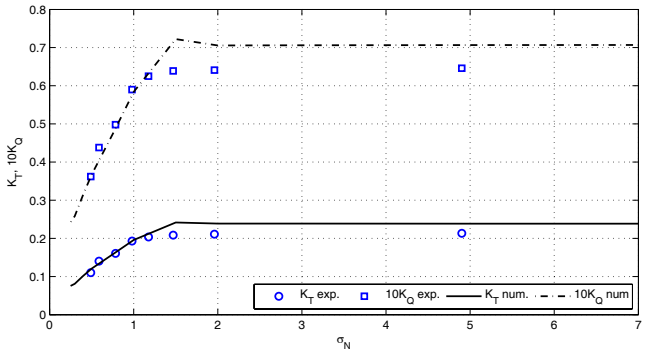

Figure 21: Newton Rader 071, P/D 1.66, J =1.4

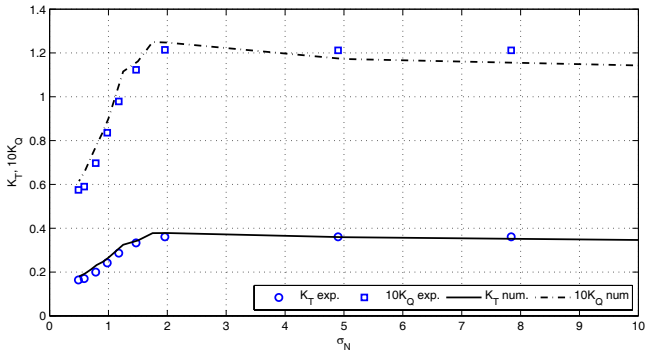

Figure 22: Newton Rader 071, P/D 2.06, J =1.4

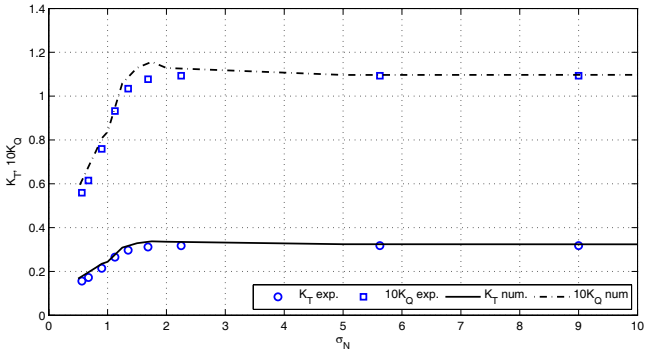

Figure 23: Newton Rader 071, P/D 2.06, J =1.5

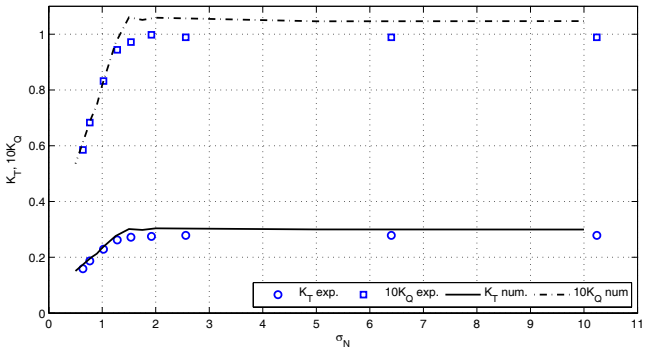

Figure 24: Newton Rader 071, P/D 2.06, J =1.6

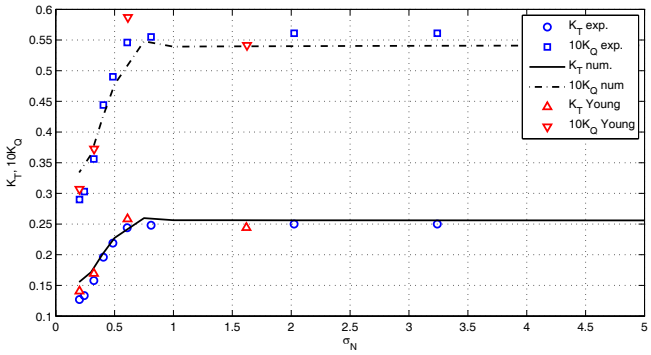

Figure 25: Newton Rader 095, P/D 1.24, J =0.9

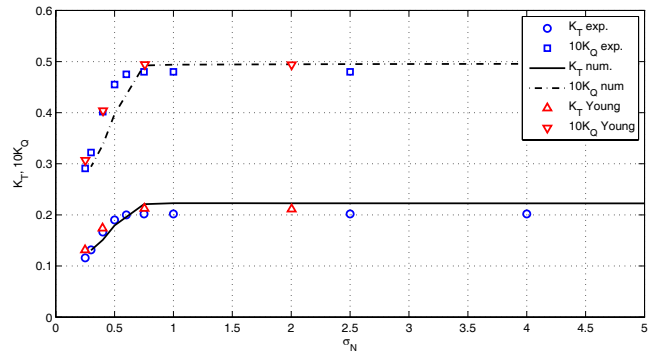

Figure 26: Newton Rader 095, P/D 1.24, J =1.0

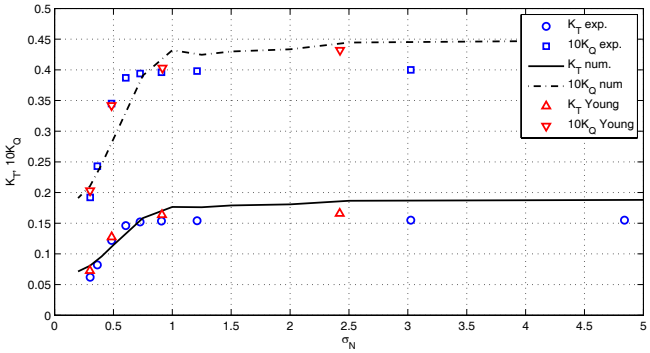

Figure 27: Newton Rader 095, P/D 1.24, J =1.1

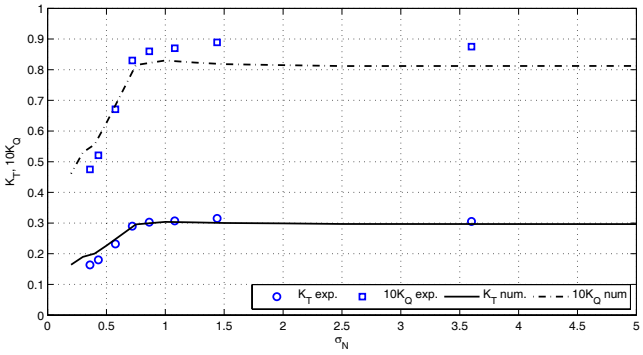

Figure 28: Newton Rader 095, P/D 1.65, J =1.2

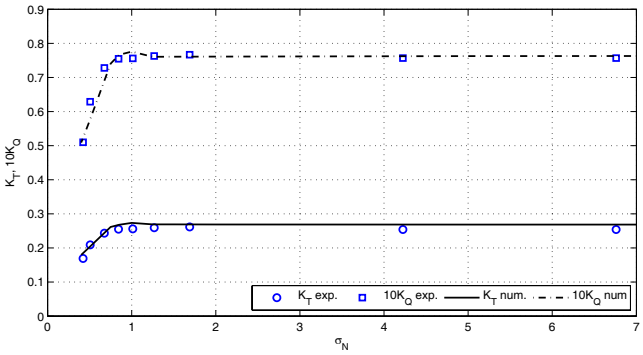

Figure 29: Newton Rader 095, P/D 1.65, J =1.3

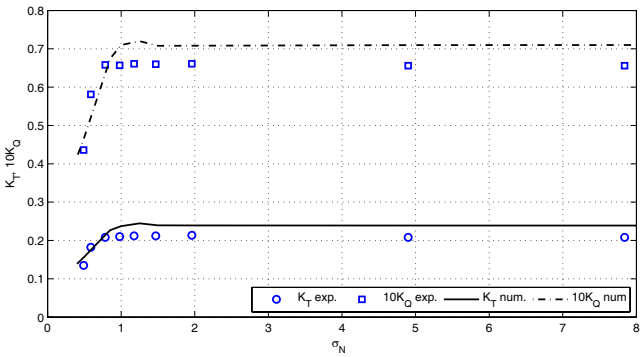

Figure 30: Newton Rader 095, P/D 1.65, J =1.4

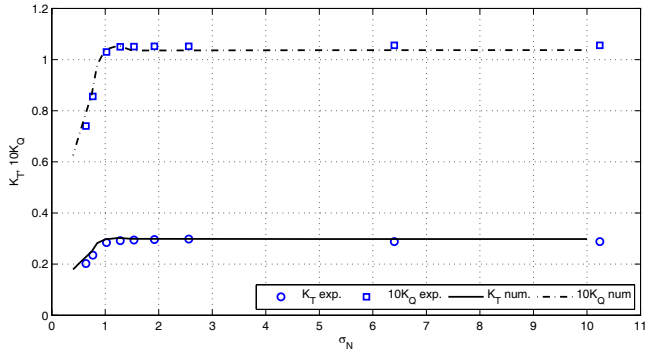

Figure 31: Newton Rader 095, P/D 2.04, J =1.6

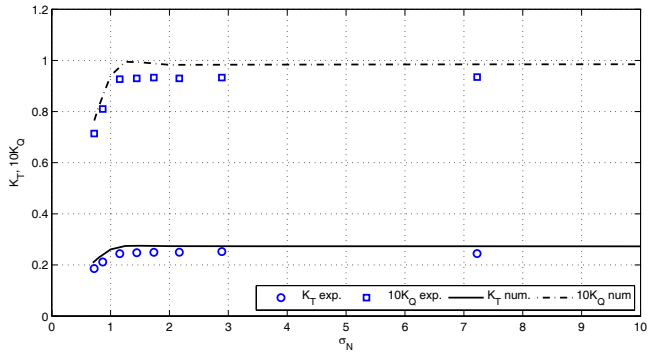

Figure 32: Newton Rader 095, P/D 2.04, J =1.7

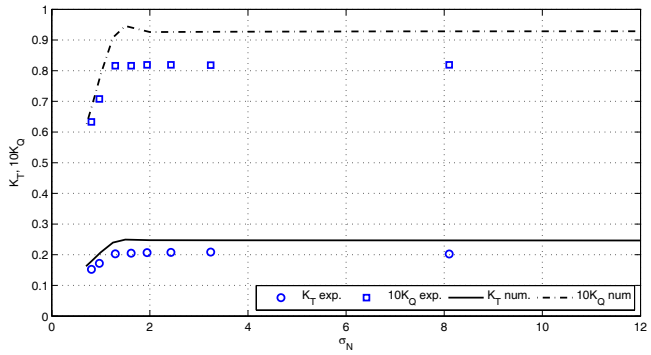

Figure 33: Newton Rader 095, P/D 2.04, J =1.8

The experimental values and the numerical computations of thrust and torque, as shown from figure 10 to figure 33, in which the lines represent the numerical solutions and the dots the experimental measures (unless otherwise specified), compares, generally, well. Some discrepancies, for almost all the geometrical configuration tested, are, however, present, specially for high (with respect to the design advance coefficient) values of advance coefficient. The predicted thrust and torque coefficient for the parent propeller and for the propeller A3/95/124 are very close to the numerical computations performed by Young and Liu, (2008) [17] with PROPCAV, a Boundary Element Method based on the same approach of the devised code and with the same capabilities (plus more others, like tip vortex cavitation and the blunt trailing edge options that are still in development in our numerical tool), so similar conclusion and justification for the discrepancies can be drawn.

In fully wetted condition, with the increase of advance coefficient, the thrust and torque coefficients are overpredicted (see, for instance, the performance of propeller A3/48/167 at J=1.4, A3/48/206 at J=1.6, A3/71/125 at J=1.1, A3/71/166 at J=1.4, A3/71/206 at J=1.6, A3/95/124 at J=1.1 and A3/95/204 at J=1.8). In cavitating condition the thrust and torque breakdown are better captured, but increasing the advance coefficient and lowering the cavitation index some differences can be highlighted with respect to the experimental measures. At low cavitation indexes the predicted thrust and torque coefficients, specially for the propeller with lower value of pitch over diameter ratio, are under predicted, and also this drawback of the numerical code is in accordance with the others numerical computations found in literature.

The simplifying hypothesis on which the potential panel method is based could be the reasons of these discrepancies. For the solution of the problem, the force free condition on the trailing wake is only approximated. The trailing wake, following the work by Salvatore, (2004) [13] is approximated with an helical surface whose pitch is a weighted average between the hydrodynamic and the blade pitch at each radial position. A more consistent wake alignment scheme (like that proposed by Pyo and already included in the steady non cavitating version of the developed code, as in Gaggero and Brizzolara, (2007) [5]) should be included to correctly model the wake at very high values of advance coefficient, and an iterative scheme should be employed to capture the non linear effects between wake position and back and face cavitation at very low values of cavitation index.

Moreover, at very high values of advance coefficient and in severe cavitating conditions, the viscous and turbulence effects (neglected by a potential solver) could be significant, for the alignment of the wake itself but also for the computation of face and back cavity detachment points. With the hypotheses of an irrotational, incompressible and inviscid fluid, the viscous effects are included only via standard viscous corrections, by means of friction coefficients applied on the wetted part of the blades. All the influence of the vortical structures and of the boundary layers on the development of the cavity is neglected: at high values of advance coefficient, as shown in figure 39, back midchord supercavitation and partial face cavitation are present on the blade at the same time and, even if in the present method midchord cavitation is treated with the same hypotheses of sheet cavitation, generally midchord cavitation leads to bubble cavitation, with a different dynamics on the performance of the propeller.

Cavitation, moreover, is an intrinsic unsteady phenomenon also if the propeller is tested in steady, uniform flow. If, for high speed, supercavitating propellers are suitable because they move the cavity closure point well aft on the wake instead than on the blade, reducing erosion and granting more stable performances, in the case of midchord cavitation the unsteadiness, not captured by a simple sheet cavity model, together with the risk of bubble cavitation, could plays an important role.

The analysis of the cavity planform of the tested propellers further highlight some of the peculiarities of Newton Rader propellers working in cavitating conditions.

As experimentally observed and reported in the work by Newton and Rader, face cavitation characterize model propellers with pitch over diameter around 1.25 (exactly 1.25 for the parent propeller, 1.24 for the A3/95 propeller family) for advance coefficients greater than about 1.0.

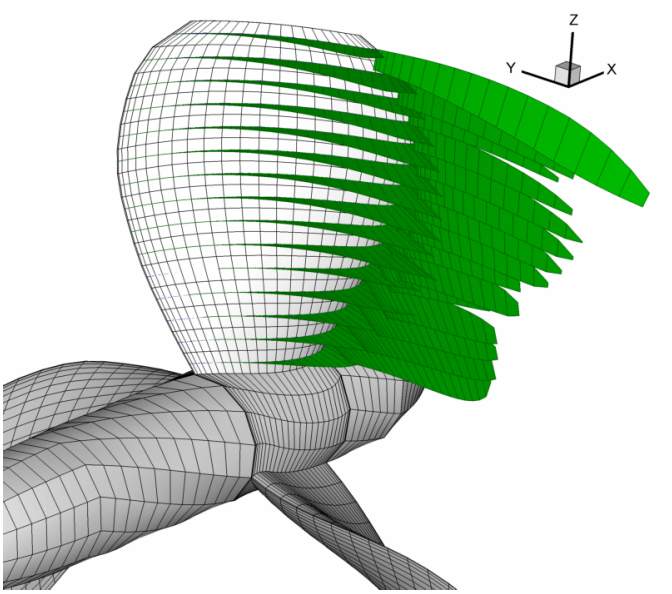

Figure 34: Back cavitation, Newton Rader 048, P/D 2.08, J =1.5, $\sigma_V = 0.25$

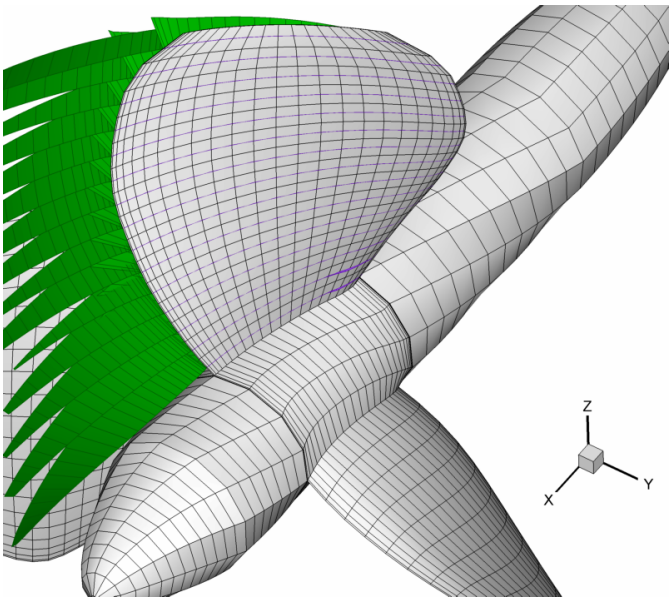

Figure 35: Face cavitation, Newton Rader 048, P/D 2.08, J =1.5, $\sigma_V = 0.25$

Also numerically this trend is verified. Almost in all the tested working condition the propellers are characterized by back midchord supercavitation (see, for instance, figure 34) and face leading edge cavitation when the advance coefficient is enough high (i.e. the angle of attack is locally negative, as in figure 39). As presented in figure 39 and 41, for J equal to 1 and to 1.1 the parent propeller is affected by a quite evident face cavitation (a bit overestimated with respect to the experimental measures and the numerical analysis by Young, (2008) [17]), that become stronger lowering the cavitation index.

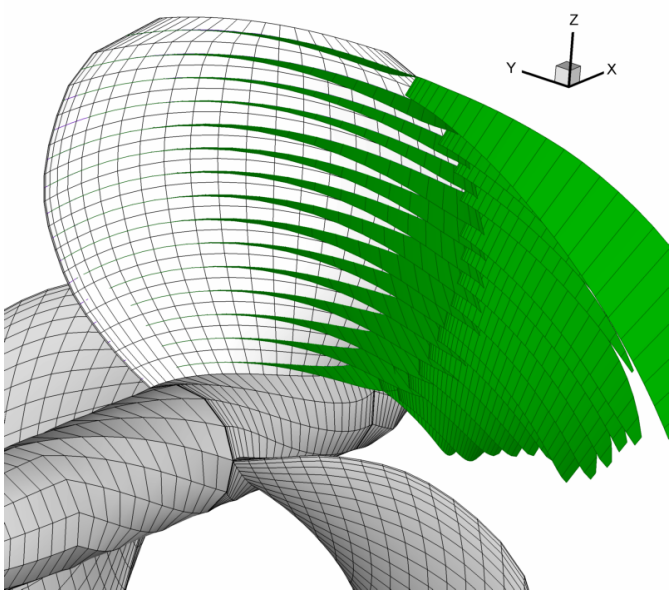

Figure 36: Back cavitation, Newton Rader 071, P/D 1.25, J =0.9, $\sigma_V = 0.25$

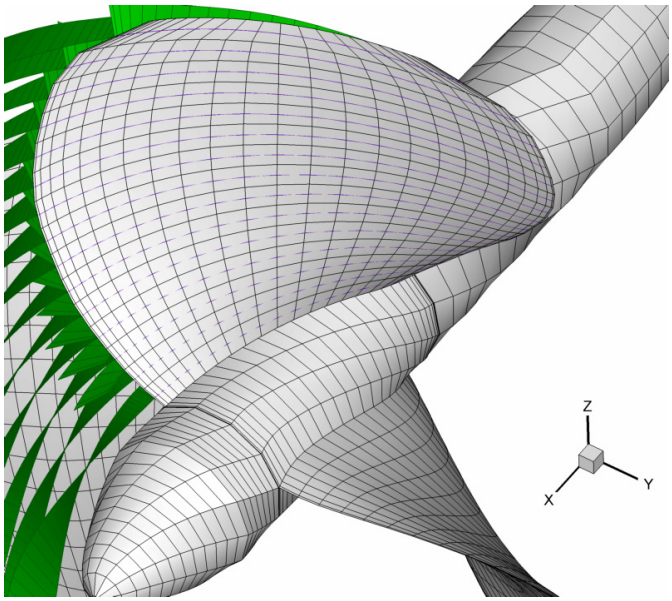

Figure 37: Face cavitation, Newton Rader 071, P/D 1.25, J =0.9, $\sigma_V = 0.25$

With respect to the same working condition (J=1, σ_V = 0.25) the face cavitation that affects propeller A3/95/124 (figure 43) is less evident and, as suggested by Young, this could be responsible of the better performance, in cavitating conditions, of the propeller with 0.95 BAR. Same conclusion holds in the case of J=1.1 and σ_V = 0.40. The A3/71/125 propeller (figure 41) has a face cavity less "evident" with respect to the face cavity of propeller A3/95/124 of figure 45 but, percentually, the

extension of the face cavity along the chord is greater for the A3/71/125 propeller, reducing its performance with respect to the same configuration but with BAR equal to 0.95. The most important effect of the blade area ratio can be, as expected, recognized in cavitating conditions: while, in fully wetted flow, the interference between blades and the viscous effects penalizes propellers with the greater blade area ratio, in cavitating flow the better performances can be achieved when the face cavitation is less relevant with respect to the wetted area, that is greater for propeller with higher BAR values.

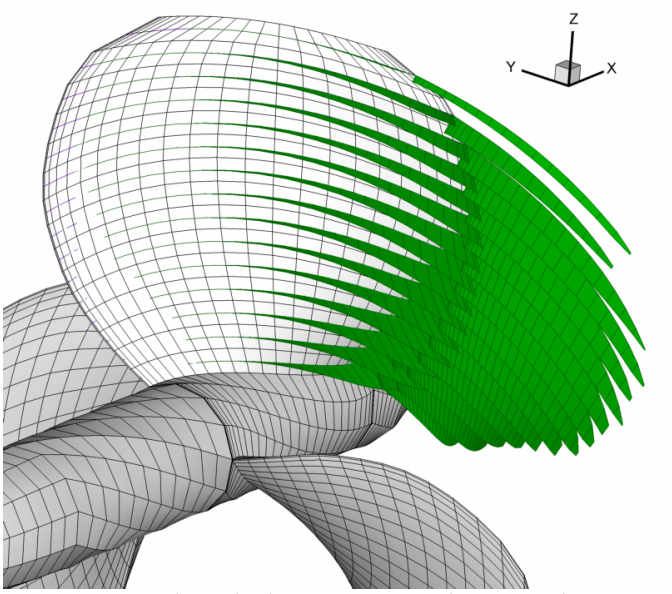

Figure 38: Back cavitation, Newton Rader 071, P/D 1.25, J =1.0, $\sigma_V = 0.25$

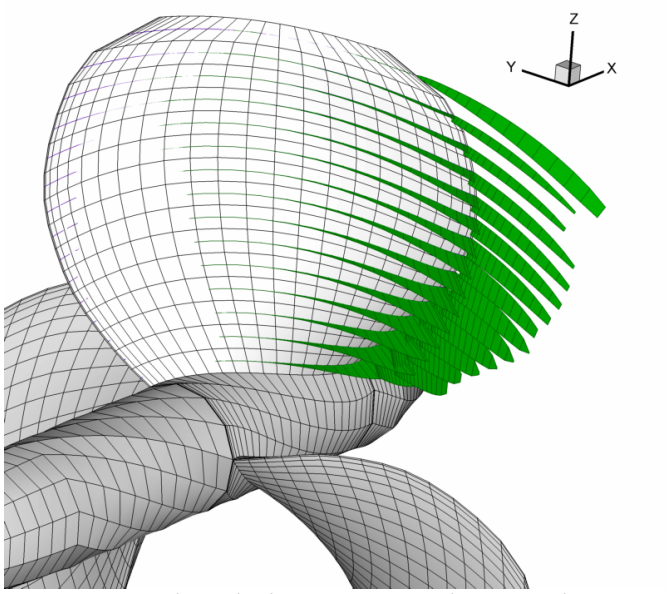

Figure 40: Back cavitation, Newton Rader 071, P/D 1.25, J =1.1, $\sigma_V = 0.40$

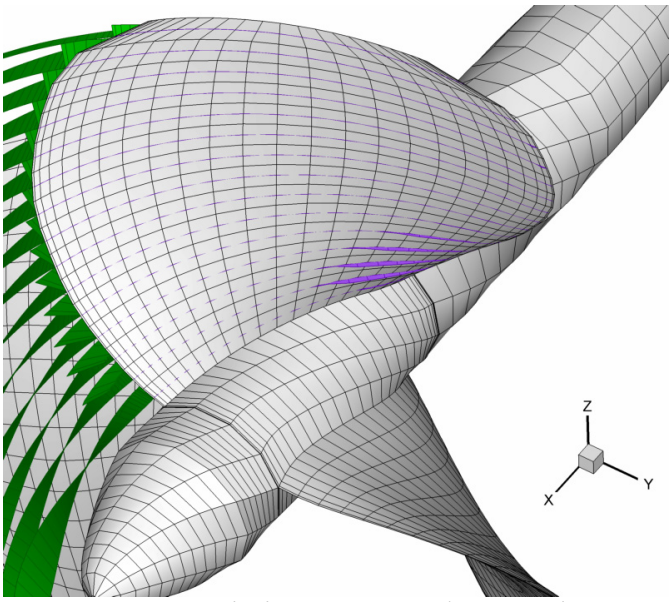

Figure 39: Face cavitation, Newton Rader 071, P/D 1.25, J =1.0, $\sigma_V = 0.25$

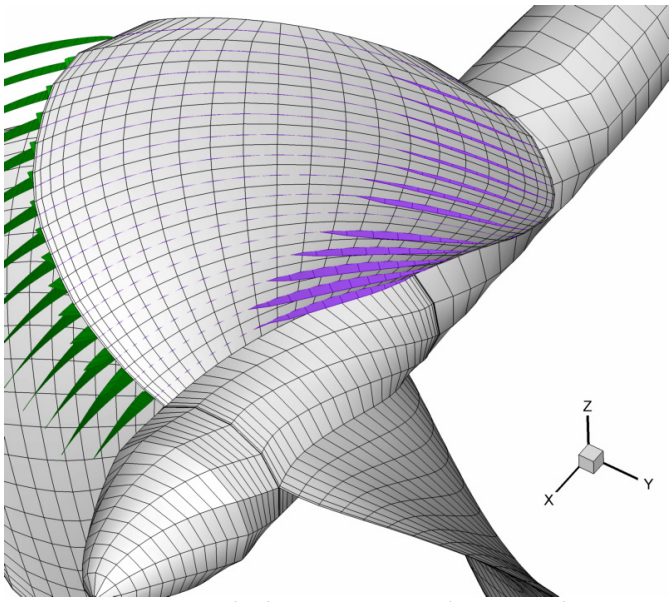

Figure 41: Face cavitation, Newton Rader 071, P/D 1.25, J =1.1, $\sigma_V = 0.40$

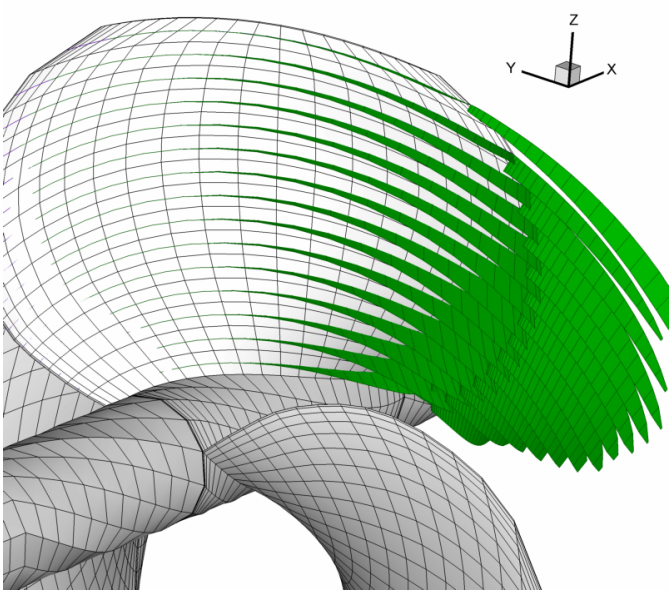

Figure 42: Back cavitation, Newton Rader 095, P/D 1.24, J =1.0, $\sigma_V = 0.25$

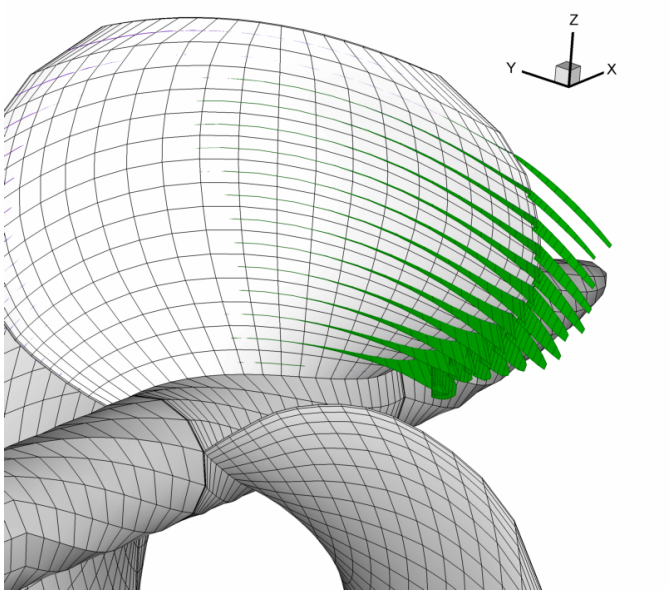

Figure 44: Back cavitation, Newton Rader 095, P/D 1.24, J =1.1, $\sigma_V = 0.40$

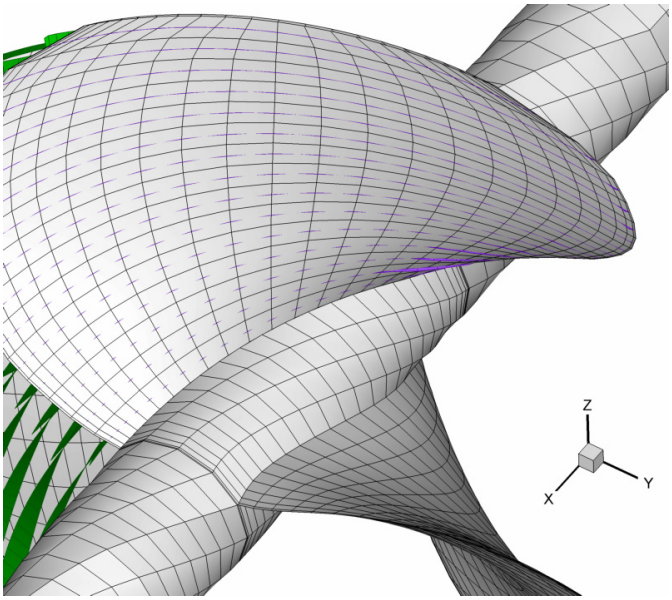

Figure 43: Face cavitation, Newton Rader 095, P/D 1.24, J =1.0, $\sigma_V = 0.25$

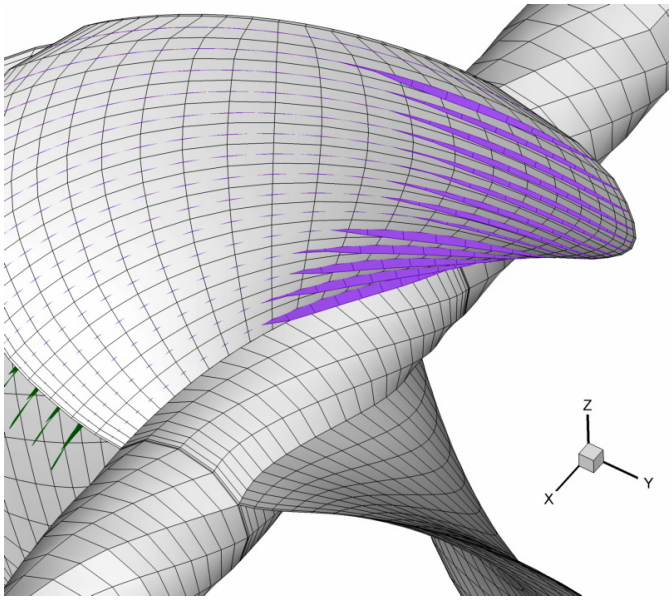

Figure 45: Face cavitation, Newton Rader 095, P/D 1.24, J =1.1, $\sigma_V = 0.40$

CONCLUSION

The Boundary element method, developed at the University of Genova, has been extended in order to deal with suction side supercavitation in junction with contemporary face leading edge sheet cavitation. Theoretical and numerical details of the solution algorithm employed to solve steady potential flow on three dimensional lifting bodies, such as hydrofoils and propellers, have been presented in the paper. The accuracy and convergence of the method have been presented and discussed in the case of supercavitating three dimensional hydrofoils, showing good correlation with similar numerical simulations.

The application of the method, in case of a propeller designed with standard NACA profiles as the propeller E033, evidenced excellent correlation with experimental results in terms of predicted cavity planform shape.

Experimental validation studies, carried out on the complete series of Newton-Rader model propellers, evidence the ability of the devised code to capture quite well the propellers performances in very different working conditions, like subcavitating regime, partially cavitating and supercavitating conditions, even if with face cavitation. The agreement is excellent for advance coefficients around the design advance coefficient (0.993 for the parent propeller) for a wide range of different cavitation indexes, while a general overestimation can be recognized in off design condition, specially at higher values of advance coefficient.

Instead, the thrust and torque breakdown, corresponding to lower values of cavitation index, are always well predicted: with a fully developed super cavity bubble on the suction side, the performance of the propeller mostly depends only on the profile face geometry (because the back side has a pressure fixed to the vapour tension) and of its pressure distribution that is, generally, well computed. Moreover, it has been demonstrated that the face leading edge cavitation (that the current method tends to overestimate) plays an important role in reducing cavitating propeller performance and that should be avoided (for instance increasing blade area ratio or modifying blade leading edge, as already done by Newton and Rader but, probably, not sufficiently) in order to obtain good multispeed performances.

Also the cavity planforms, at different cavitation indexes, qualitatively agree with the computed supercavity that are, instead, quite similar to the other numerical cavity shape available in literature.

Further developments of the present method currently planned are the extension of the numerical scheme to treat face supercavitation together with arbitrary points supercavity detachment, in order allow the code to solve finite trailing edge profiles. Finally, the supercavity model has to be included in the unsteady potential solver, allowing the computation of unsteady, supercavitating propellers performances.

REFERENCES

[1] Caponnetto, M. and Brizzolara, S. 1995, "Theory and Experimental Validation of a Surface Panel Method for the Analysis of Cavitating Propellers in Steady Flow", *PROPCAV'95 Conference*.

[2] Brizzolara, S., Gaggero, S. and Grasso, A. 2009, "Parametric Optimization of Open and Ducted Propellers", *to appear on the Proceedings of the SNAME Propellers and Shafting Symposium*.

[3] Dang, J. and Kuiper, G. 1999, "Re-entrant Jet Modeling of Partial Cavity Flow on Three Dimensional Hydrofoils", *Journal of Fluid Engineering,* vol. 121.

[4] Fine, N.E. 1992, "Non linear Analysis of Cavitating Propellers in Nonuniform Flow", *Phd. Thesis, M.I.T. Department of Ocean Engineering*.

[5] Gaggero, S. and Brizzolara, S. 2007, "Exact Modeling of Trailing Vorticity in Panel Methods for Marine Propellers", *2nd International Conference on Marine Research and Transportation,* D-1, D-9.

[6] Gaggero, S. and Brizzolara, S., 2008, "A Potential Panel Method for the Analysis of Propellers in Unsteady Flow", *8th International Symposium on High Speed Marine Vehicles*, vol. 1, 115-123.

[7] Gaggero, s. and Brizzolara, S. 2008, "A Potential Panel Method for the Prediction of Midchord face and back Cavitation", *6th International conference on High Performance Marine Vehicles,* vol. 1, 33-46.

[8] Gaggero, S. and Brizzolara, S. 2009, "Parametric CFD Optimization of Fast Marine Propellers", *to appear on the Proceedings of the 10th International Conference on Fast Sea Transportation FAST2009*.

[9] Lee, J.T. 1987, "A Potential Based Panel Method for the Analysis of Propellers in Steady Flow", *Phd. Thesis, M.I.T. Department of Ocean Engineering*.

[10] Morino, L. and Kuo, C.C. 1974, "Subsonic Potential Aerodynamics for Complex Configuration: a general theory", *AIAA Journal,* vol.12, 191-197.

[11] Mueller, A.C. and Kinnas, S.A. 1999, "Propeller Sheet Cavitation Predictions Using a Panel Method", *Journal of Fluids Engineering*, vol. 121.

[12] Newton, R. and Rader, H. 1961, "Performance Data of Propellers for High Speed Crafts", *Transactions of the Royal Institution of Naval Architects,* 103, 93-129.

[13] Pereira, F., Salvatore, F. and Di Felice, F. 2004, "Measurements and Modeling of Propeller Cavitation in Uniform Inflow", *Journal of Fluid Engineering,* vol. 126.

[14] Tachmindji, A.J. and Morgan, W.B. 1957, "The Design and Performance of Supercavitating Propellers", *DTMB Report AD0145521*.

[15] Vaz, G. and Bosschers, J. 2006, "Modelling Three Dimensional Sheet Cavitation on Marine Propellers Using a Boundary Element Method", *6th International Symposium on Cavitation*.

[16] Young, Y.L. and Kinnas, S.A. 2001, " A BEM for the Prediction of Unsteady Midchord Face and/or Back Propeller Cavitation", *Journal of Fluids Engineering,* vol. 123.

[17] Young, Y.L. and Liu Z. 2008 "Performance Prediction of Newton Rader Propellers", *Journal of Ship Research,* 52,2 124-145.

[18] Young, Y.L. 2002, "Numerical Modeling of Supercavitating and Surface Piercing Propellers", *Phd. Thesis, The Environmental and Water Resource Engineering Department of Civil Engineering, The University of Texas at Austin*.

[19] Young, Y.L. and Kinnas, S.A. 2001, "Numerical Modeling of Supercavitating and Surface Piercing Propeller Flows", *4th International Symposium on Cavitation*.

[20] Young, Y.L. and Kinnas, S.A. 2004, "Performance Predictions of Surface Piercing Propellers", *Journal of Ship Research,* 48, 288-304.